Chinese Journal of Mechanical Engineering

ORIGINAL ARTICLE

Open Access

Effects of Orthogonal Heat Treatment on Microstructure and Mechanical Properties of GN9 Ferritic/Martensitic Steel

Tingwei Ma[1,2], Xianchao Hao[3*] and Ping Wang[1*]

Abstract

Microstructure and mechanical properties of GN9 Ferritic/Martensitic steel for sodium- cooled fast reactors have been investigated through orthogonal design and analysis. Scanning electron microscopy (SEM), transmission electron microscopy (TEM), differential scanning calorimeter (DSC), tensile and impact tests were used to evaluate the heat treatment parameters on yield strength, elongation and ductile-to-brittle transition temperature (DBTT). The results indicate that the microstructures of GN9 steel after orthogonal heat treatments consist of tempered martensite, $M_{23}C_6$, MX carbides and MX carbonitrides. The average prior austenite grains increase and the lath width decreases with the austenitizing temperature increasing from 1000 °C to 1080 °C. Tempering temperature is the most important factor that influences the dislocation evolution, yield strength and elongation compared with austenitizing temperature and cooling methods. Austenitizing temperature, tempering temperature and cooling methods show interactive effects on DBTT. Carbide morphology and distribution, which is influenced by austenitizing and tempering temperatures, is the critical microstructural factor that influences the Charpy impact energy and DBTT. Based on the orthogonal design and microstructural analysis, the optimal heat treatment of GN9 steel is austenitizing at 1000 °C for 0.5 h followed by air cooling and tempering at 760 °C for 1.5 h.

Keywords Ferritic/Martensitic steel, Orthogonal design, $M_{23}C_6$ carbide, Ductile-to-brittle transition temperature

1 Introduction

Compared with austenitic stainless steels, 9%–12%Cr heat-resistant steels exhibit superior resistance to radiation-induced swelling [1], high thermal conductivity and low thermal expansion [2]. They also have good oxidation and corrosion resistance in liquid metals at elevated temperatures [3, 4]. Hence, 9%–12%Cr steels are considered as one of the main candidate materials for core structures in Generation IV nuclear reactors [2, 5]. From 1950's, three generations of heat-resistant steels have been manipulated in fossil power plants [6, 7]. Modified 9Cr-1Mo steel (commercialized as T91 steel) is the second generation heat-resistant steel. It was modified from T9 (9Cr-1Mo) steel by adding V, Nb, and N from 1970's and have been extensively used in fossil power plants [8] because of its high creep-rupture strength at 500–600 °C. For employment in high-neutron irradiation environments, modified 9Cr-1Mo steel would become sensitive to an abrupt shift in ductile-to-brittle transition temperature (DBTT) towards high temperatures and a decrease in the upper shelf energy (USE) [9–11]. As a main candidate for wrapper applications in sodium-cooled fast reactors, the increase in the DBTT and the reduction in

*Correspondence:
Xianchao Hao
xchao@imr.ac.cn
Ping Wang
wping@epm.neu.edu.cn
[1] Key Laboratory of Electromagnetic Processing of Materials, Ministry of Education, Northeastern University, Shenyang 110004, China
[2] Yingkou Institute of Technology, Yingkou 115014, China
[3] CAS Key Laboratory of Nuclear Materials and Safety Assessment, Institute of Metal Research, Chinese Academy of Sciences, Shenyang 110016, China

impact toughness is the most serious concern for application of modified 9Cr-1Mo steel. Lowering the DBTT and increasing the USE of 9%–12%Cr steels before irradiation is considered a useful method to reduce the increments of DBTT and reduction of USE [12]. Though irradiation conditions show some extent effects on the shift of DBTT [13], metallurgical conditions of 9%–12%Cr steels are considered the main influential factors. The reduction of inclusion content [14] or impurity elements [15] in ingots are effective to enhance impact toughness. The modifications of chemical composition [5, 16], microstructure [17, 18] and heat treatment [2, 19, 20] are also useful methods.

Two important steps of heat treatments, i.e., austenitizing and tempering, are performed to modify the microstructure of modified 9Cr-1Mo steel. The main microstructural evolution during austenitizing is the dissolution of carbides or carbonitrides and the transformation of martensite by following cooling. Coarsened grain size and high level of δ-ferrite should be avoided after austenitizing [21]. Microstructural evolution during tempering is complicated and involves the precipitation of carbides or carbonitrides, the modification of precipitate distribution and the annealing of dislocations. The heat treatment regime for modified 9Cr-1Mo steel recommended in literature [22–24] is austenitizing at 1040–1080 °C and tempering at 730–780 °C followed by air cooling. The resulting microstructure is composed by lath martensite and the precipitates are $M_{23}C_6$ and MX. Liu et al. [25] reported that the precipitation of M_3C depends on the cooling rate though different austenitizing temperature and cooling methods. Jones et al. [26] found that the lath structure of air-cooled was clearer than that of water quenching after austenitizing of 9Cr-1Mo steel. Grain refinement through a double austenitizing treatment and grain boundary engineering to overcome the reduction of impact toughness [5, 19].

In addition to prior austenite grain size, heat treatments have effects on precipitate characteristics, martensite lath and packet size, and dislocation character. They all show some effects on impact toughness [27, 28]. Though many studies of modified 9Cr-1Mo steel have been carried out and focused on sole parameter of heat treatments [2, 19, 20], austenitizing, tempering and the cooling methods have interactive effects on microstructure evolution and the related mechanical properties. Hence, it deserves some further research to clarify the relationship between its complex microstructure [29] and heat treatment parameters and to enhance the impact toughness. Moreover, more strict requirements have been proposed with the developments of Generation IV nuclear reactors. Modified 9Cr-1Mo steel for application in new-generation sodium-cooled reactors should have high-tensile strength, moderate ductility under ambient and elevated temperatures and low DBTT and high impact toughness [30]. To separate their effects on yield strength, elongation and ductile-brittle transition temperature (DBTT), the orthogonal design method, is used in this paper. An optimal heat treatment is, therefore, put forward based on the experimental results.

2 Materials and Experimental Procedures

2.1 Materials and Specimen Preparation

The GN9 Ferritic/Martensitic steel used in the present study was melted in a 50 kg vacuum induction furnace. The ingot was hot forged into 40 mm-thick plates and then hot-rolled into 14 mm-thick plates at 1050 °C. The chemical composition in weight percentage (wt.%) of the experimental material is listed in Table 1. The impurity contents of P, O and S are 0.009%, 0.003% and 0.003%, respectively.

The critical transformation temperature was studied by differential scanning calorimeter (DSC). From DSC result, the phase transformation temperatures, i.e., A_{c1}, A_{c3} and T_c were determined to be 822, 892 and 752 °C, respectively. Based on the obtained critical temperatures and heat treatment parameters by Gutierrez [24], the austenitizing and tempering temperatures, as well as the following cooling method after austenitizing were chosen as orthogonal factors to design the orthogonal experiment, which are presented in Table 2. Through orthogonal experiment it can obtain the optimal influence factor and parameter of GN9 steel only by few experiments. Here, *A*, *B* and *C* in Table 2 stand for austenitizing temperature, tempering temperature and cooling method, respectively. The holding time for austenitizing and tempering is 0.5 h and 1.5 h, respectively. And the cooling method after tempering is air cooling.

2.2 Microstructure and Mechanical Property Analysis

A variety of techniques, including optical microscopy (OM: Axio Observer ZIm), scanning electron microscopy (SEM: Zeiss Ultra55) and transmission electron microscopy (TEM: JEOL 2100) were employed to

Table 1 Chemical composition of GN9 steel (wt.%)

C	Si	Mn	Cr	Mo	V	Nb	N	B	Ni	Fe
0.086	0.25	0.47	8.13	0.85	0.19	0.07	0.105	0.002	0.19	Bal.

Table 2 Factors for orthogonal experiments in the present study

Experimental No.	*A* (°C)	*B* (°C)	*C*
0W	1000	650	WQ
0O	1000	700	OQ
0A	1000	760	AC
5O	1050	650	OQ
5A	1050	700	AC
5W	1050	760	WQ
8A	1080	650	AC
8W	1080	700	WQ
8O	1080	760	OQ

Note: WQ-water quenching; OQ-oil quenching; AC-air cooling.

characterize the microstructure of GN9 steel. The samples were mounted, polished and etched with a 35 g $FeCl_3$/10 mL HCl/100 mL H_2O solution for OM and SEM analysis. Five OM images were captured continuously at a magnification of 500 × for each sample and the prior austenite grain size was measured by the linear intercept method. To confirm the distribution and morphology of carbides, the samples were observed by SEM. Five images in different areas of each specimen were captured. About 100–200 carbide particles are counted and the average particle size was analyzed at a magnification of 30000 ×. Thin foils for TEM analysis were prepared by using a twin-jet electro-polishing with a polishing electrolyte containing 10 mL perchloric acid and 90 mL ethanol under the conditions of 45 mA, between − 18 and − 25 °C, and 15 cm^3/s flow rate.

Standard Charpy V-notch specimens with dimension of 10 mm × 10 mm × 55 mm (length) were machined from the tempered specimens and used for impact tests. Three specimens for each impact test were taken from hot-rolled plates in T-L direction and the results were screened and averaged. Impact tests were conducted at temperatures between − 110 °C and 23 °C. Boltzmann curves were used for analyzing the DBTT and upper shelf energy (USE).

Cylindrical tensile samples with 5 mm diameter and 25 mm gauge length were machined after tempering with gauge length parallel to rolling direction of the plate. Tensile tests were performed at room temperature and strain rate of 3×10^{-3} s^{-1} on a hydraulic test system (Hitachi 100 kN machine). Two specimens were prepared for tensile tests and the results were averaged.

3 Results

3.1 Microstructure

The microstructure of the hot-rolled specimen consists of deformed martensite and discrete carbides as shown in Figure 1(a). Austenization at 1050 °C and 1080 °C provide a structure of martensite and is marked by the absence of carbides, while austenization at 1000 °C results in a structure of martensite and undissolved carbides as shown in Figure 1(b).

The prior austenite grain size was calculated indifferent heat treatment conditions and the result is shown in Figure 2. When the austenitizing temperature increases from 1000 °C to 1080 °C, the average grain size varies from about 8 μm to about 12 μm and the prior austenite grains show sluggish growth tendency.

The microstructures of modified GN9 steel specimens in tempered conditions are analyzed using SEM and the results are shown in Figure 3. It can be seen that the amount of carbides increases with the increments of austenitizing and tempering temperatures. The carbide distribution is also influenced by heat treatment parameters. As shown in Figure 3(a), (d) and (g), carbides mainly distributed at prior austenite grain boundaries in samples tempered at 650 °C. Fine, discrete carbides precipitated at lath boundaries with the tempering temperature increasing from 650 °C to 700 °C in Figure 3(b), (e) and (h). Dense carbides distribute at boundaries of both prior austenite grains and lathes in samples tempered at 760 °C, Figure 3(c), (f) and (i). Figure 4 shows the TEM microstructure of GN9 steel after austenitizing at 1000 °C followed by air cooling and tempering at 760 °C. A typical tempered martensite laths and dense dislocations can be obviously seen with blocky carbides in chains at grain boundaries. The electron diffraction patterns in Figure 4(b) and (c) reveal that carbides in GN9 steel are $M_{23}C_6$ and MX.

From Figure 5, we can see that tempered martensite were found from 650 °C to 760 °C, the dense of dislocation in martensite laths decrease with increase of tempered temperature at the same austenitizing temperature. Blocky carbides mainly distribute at prior austenite grain boundaries and martensite lath boundaries. And fine discrete carbides present in the laths. The martensite lath width is calculated based on the TEM observations and the result is shown in Figure 2. Obviously, martensite lath width decreases from 220–250 nm to 180–190 nm with the austenitizing temperature increasing from 1000 °C to 1080 °C. Tempering show some influence on grain size and lath width, but its effect is less compared with austenitizition.

3.2 Mechanical Properties

Tensile test results of GN9 steel specimens are listed in Table 3. It is evident that the yield strength and tensile strength decrease and the elongation increase when the tempering temperature increases from 650 °C to 760 °C at the same austenitizing temperature. The increments

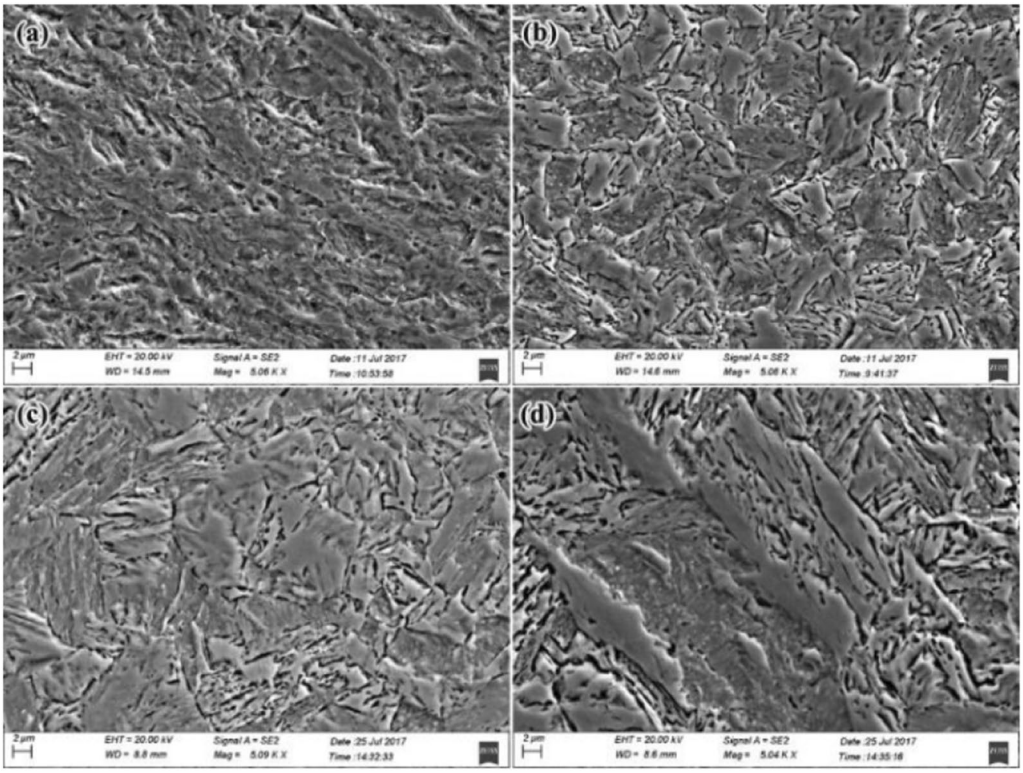

Figure 1 SEM images of GN9 steel at different condition: (**a**) Hot-rolled, (**b**) 1000 °C + AC, (**c**) 1050 °C + AC, (**d**) 1080 °C + AC

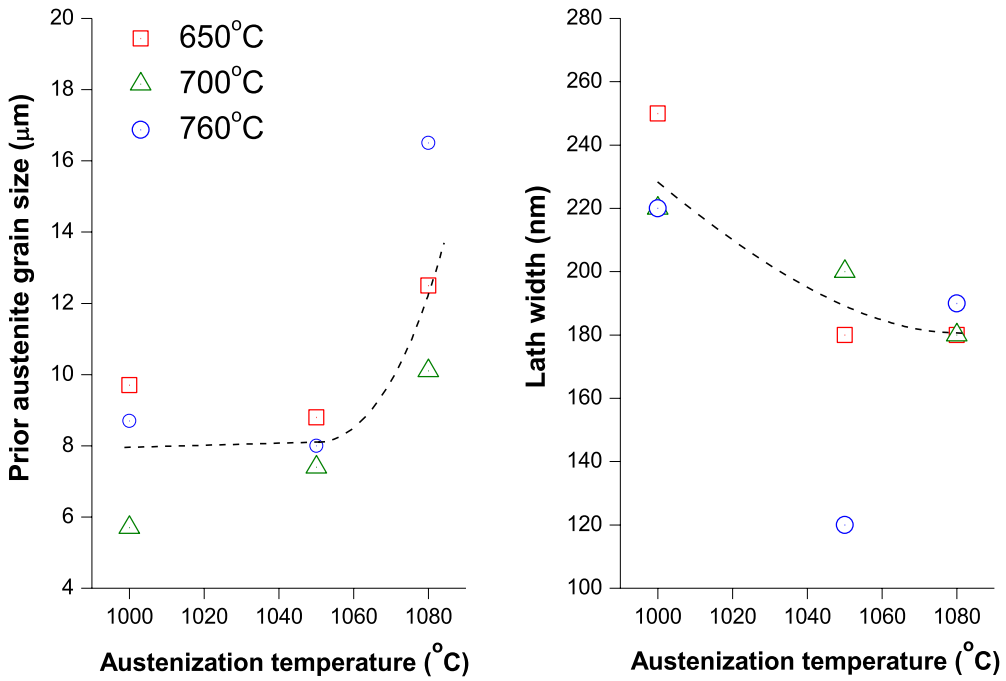

Figure 2 Prior austenite grain size of GN9 steel specimens at different heat treatment conditions

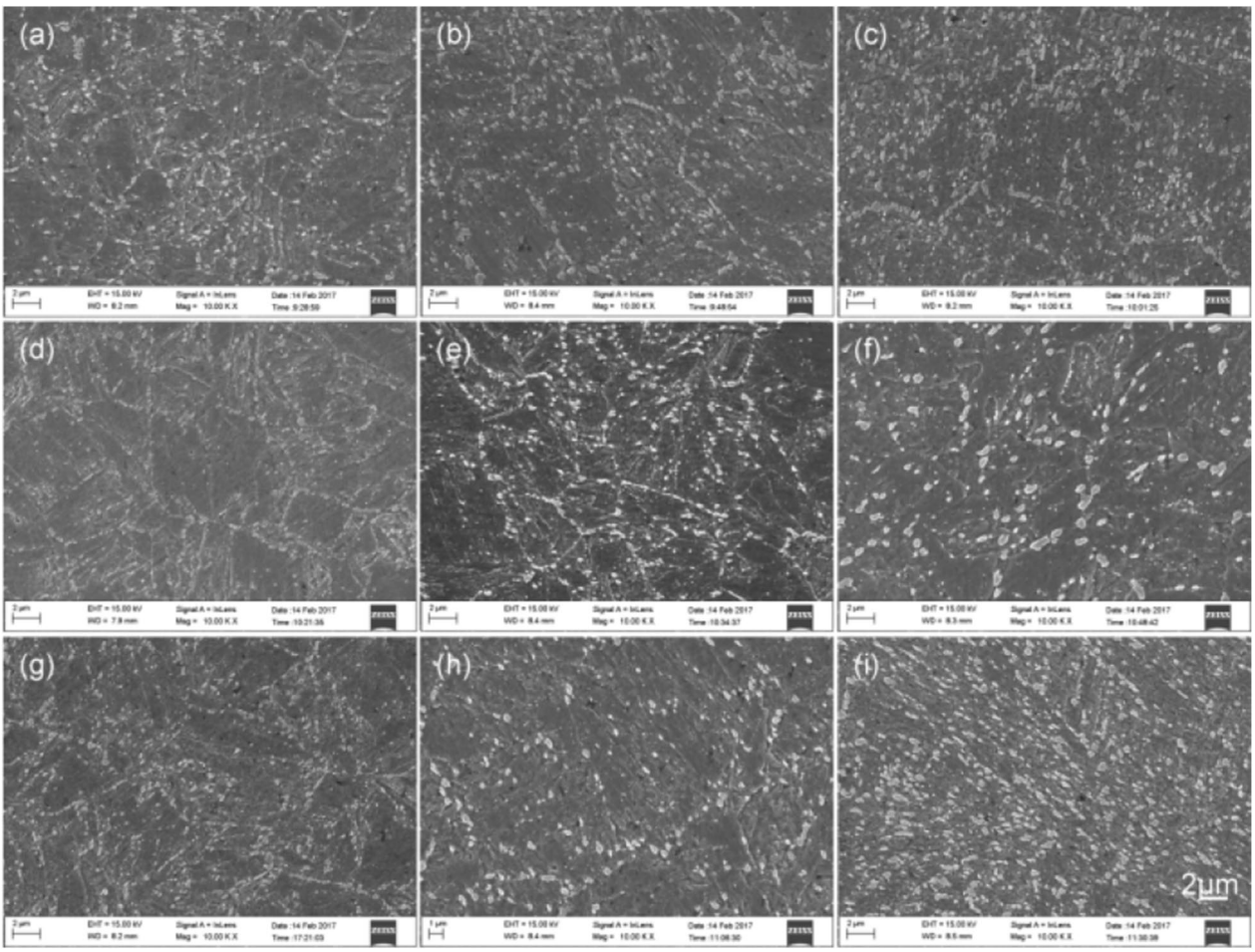

Figure 3 SEM images of carbide distribution in GN9 steel specimens at different heat treatment conditions: (**a**) 0W, (**b**) 0O, (**c**) 0A, (**d**) 5O, (**e**) 5A, (**f**) 5W, (**g**) 8A, (**h**) 8W, (**i**) 8O

of austenitizing temperature show little influence on elongation.

Figure 6 shows the temperature dependence of the impact energy of GN9 steel specimens. The upper shelf energy (USE) is obtained through Boltzmann analysis. The temperature at impact energy of the half of USE in Figure 6 is defined as DBTT and the results are listed in Table 3. We could see from Table 3 that the increment of tempering temperature could improve the USE, while austenitizing temperature shows less impact on the USE. The lower shelf energies decease with the increasing of yield strengths, but the upper shelf energies are independent of yield strength for the same tempering temperature. This trend is similar as that reported by Little [31].

3.3 Orthogonal Design Analysis

The influence of heat treatment parameters on yield strength, elongation and DBTT is analyzed by orthogonal design methods and the related factors $\overline{K_i}$ and R [32]. $\overline{K_i}$ is the mathematic average value of any column on level number i ($i = 1, 2, 3$).$\overline{K_i}$ for factor j ($j =$ A, B, C) is calculated by Eq. (1). R is a value of subtraction between the maximum and the minimum of $\overline{K_i}$ in the same factor. R for factor j is calculated by Eq. (2). The average values $\overline{K_i}$ and R value of the yield strength ($R_{p0.2}$), elongation (EL) and impact toughness (DBTT) for each factor at different levels are depicted in Tables 4, 5 and 6 and Figure 7.

$$\overline{K_{ij}} = (\overline{K_{1j}} + \overline{K_{2j}} + \overline{K_{3j}})/3, \tag{1}$$

$$R_j = \max(\overline{K_j}) - \min(\overline{K_j}), \tag{2}$$

where R manifests the relative influence on the objective functions. The higher the R, the stronger the influence of factor. Because R is subtraction between the maximum and the minimum $\overline{K_i}$ in the same factor, it can be analyzed intuitively by $\overline{K_i}$. The level of factor is important if $\overline{K_i}$ is the maximum. Take the yield strength for example,

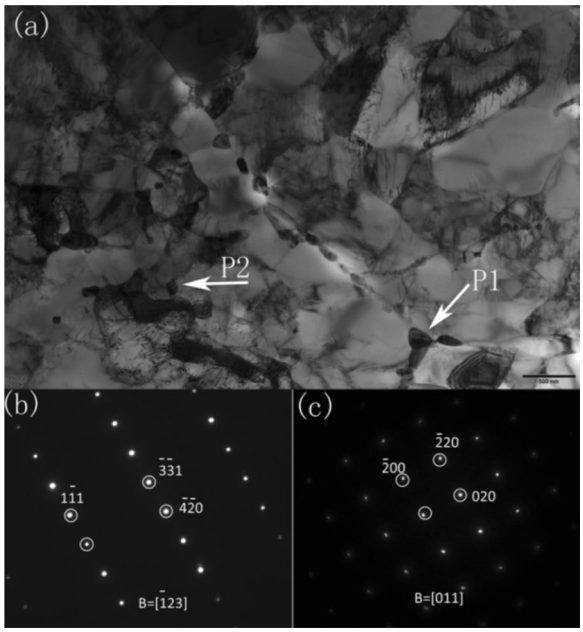

Figure 4 TEM micrographs of GN9 steel in 0A condition: (**a**) Tempered martensite laths, (**b**) $M_{23}C_6$ SAED of P1 in (**a**), and (**c**) MX SAED of P2 in (**a**)

$\overline{K_3}$ is the maximum in the factor of austenitizing temperature in Table 4, it is concluded that normalization at 1080 °C is a more important level than that at 1000 °C or 1050 °C. In terms of $\overline{K_1}$, tempering at 650 °C is a more important level than that at 700 °C or 760 °C. For $\overline{K_2}$ analysis, OQ is a more important level than WQ and AC. Analysis for EL and DBTT is performed in the same manner. As shown in Tables 5 and 6, austenitizing at 1000 °C, tempering at 760 °C and AC are important levels for EL, while austenitizing at 1000 °C, tempering at 760 °C and AC are important levels for DBTT.

For analyzing the effect of heat treatment factors on the material mechanical properties and finding out the optimum heat treatment regime, the analysis of variance (ANOVA) method was used on the basis of the degree of freedom (*f*), the sum of squares (*S*), variance (*V*), and *F*-value. In these parameters, the difference between the values at different levels of each factor represents the relative influence degree [33]. The larger the difference, the stronger the influence [34]. The formulae applied in the present study are defined in Eqs. (3)–(7):

$$f_j = m - 1, \tag{3}$$

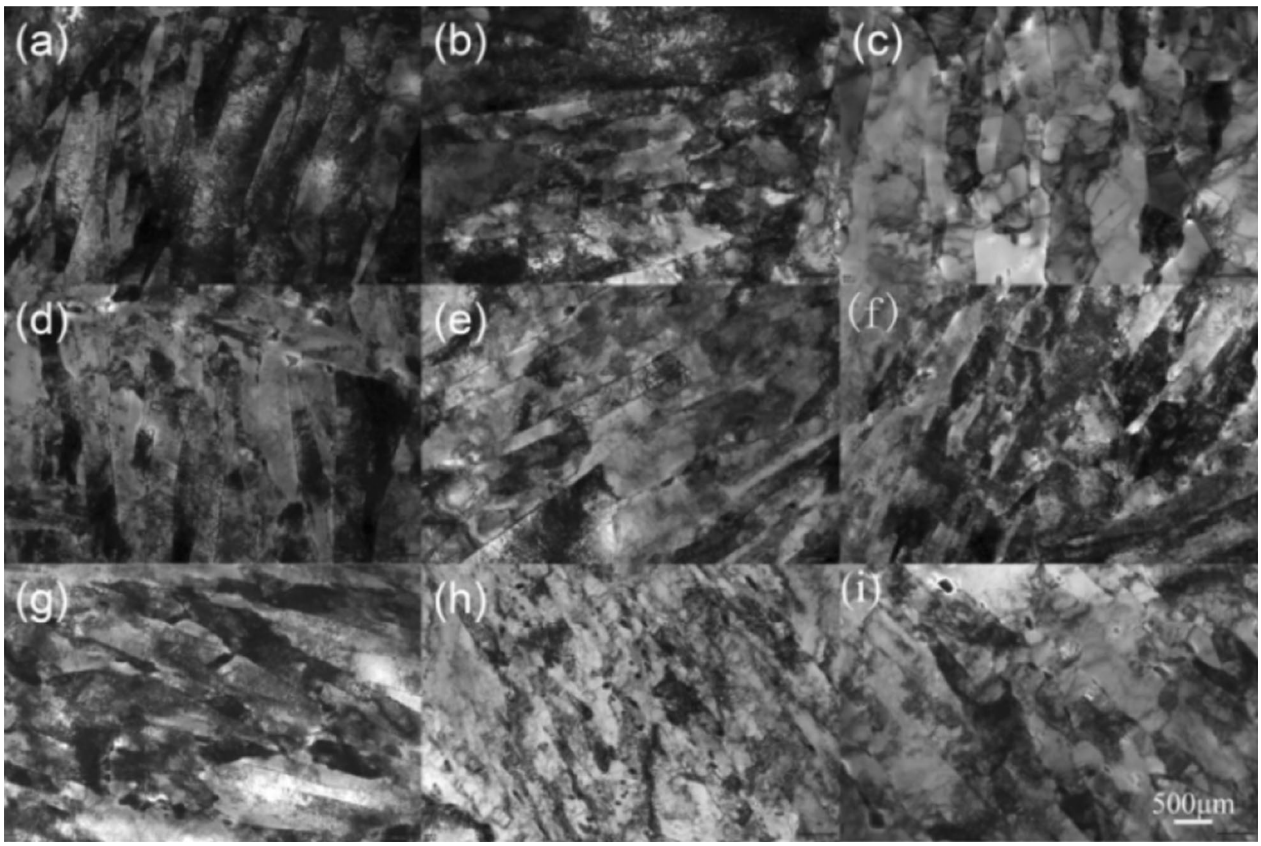

Figure 5 TEM micrographs of GN9 steel at different heat treatment conditions: (**a**) 0W, (**b**) 0O, (**c**) 0A, (**d**) 5O, (**e**) 5W, (**f**) 5A, (**g**) 8A, (**h**) 8W, (**i**) 8O

Table 3 Tensile properties of GN9 steel specimens

Experimental No.	$R_{p0.2}$ (MPa)	R_m (MPa)	EL (%)	RA (%)	DBTT (°C)	USE (J)
0W	821.5	936	20.3	69.0	− 18	172
0O	674.5	802	21.5	70.0	− 50	182
0A	523.5	710.5	26.5	68.0	− 58	216
5O	861.5	996.5	19.5	63.5	3	155
5A	723	845.5	20.3	66.0	− 28	192
5W	517	689.5	23.0	71.5	− 40	203
8A	849	971	20.0	67.0	− 26	162
8W	755	866	20.0	71.0	− 27	111
8O	580.5	729.5	23.5	72.0	− 14	198

Note: $R_{p0.2}$: yield strength, R_m: tensile strength, EL: elongation, RA: reduction of area

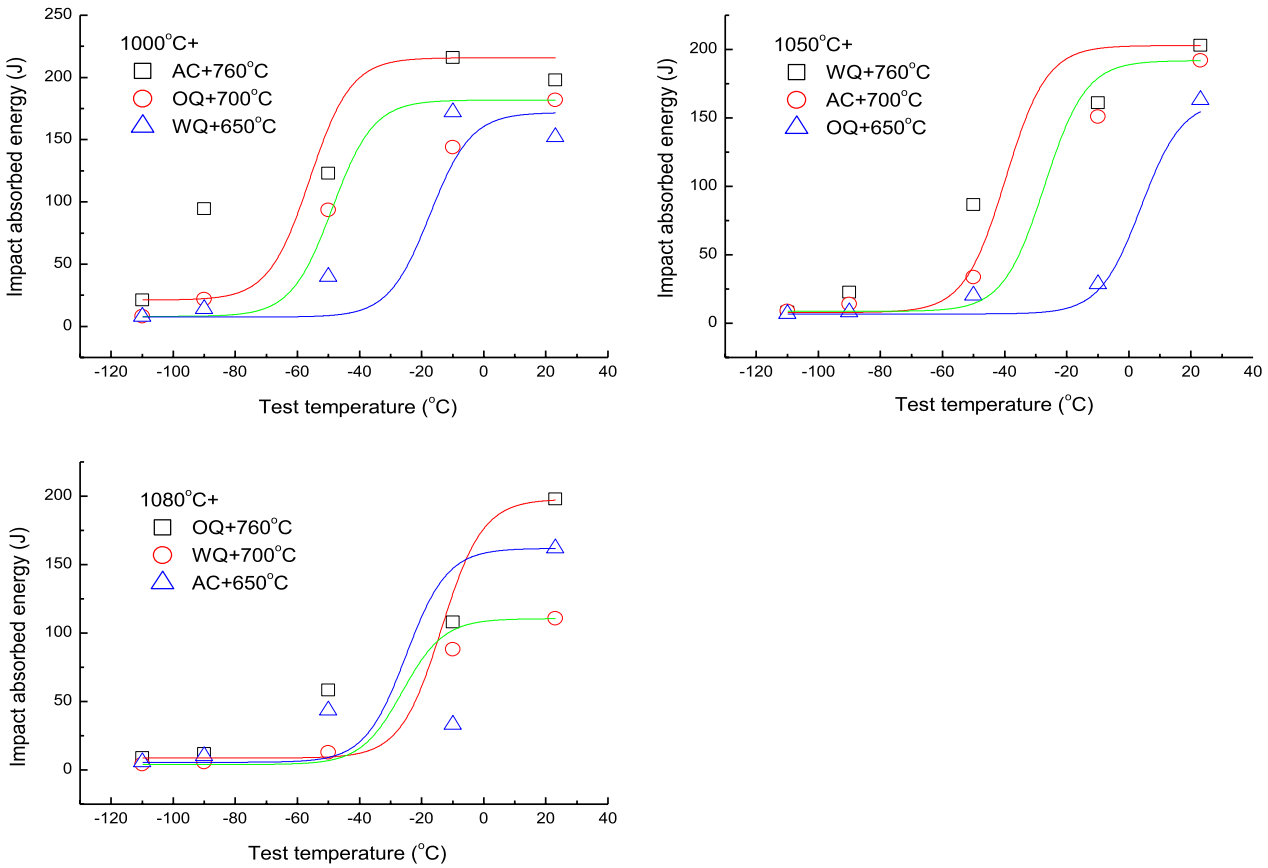

Figure 6 Correlation of Charpy impact energy, test temperature and heat treatment for GN9 steel specimens

$$S_j = \frac{1}{n}\sum_{i=1}^{m}(\sum_{j=1}^{n}K_{ij})^2 - (\sum_{i=a}^{m}\sum_{j=1}^{n}K_{ij})^2/mn, \tag{4}$$

$$S_T = \sum_{i=1}^{m}\sum_{j=1}^{n}K_{ij}^2 - (\sum_{i=a}^{m}\sum_{j=1}^{n}K_{ij})^2/mn, \tag{5}$$

$$V_j = S_j/f_j, \tag{6}$$

$$F_j = V_j/V_e = (S_j/f_j)/(S_e/f_e), \tag{7}$$

where m is the number of factors, n is the experiment number of each factor, V_e is the variance of error.

Table 4 Orthogonal design analysis of yield strength ($R_{p0.2}$)

Source	$\overline{K_1}$	$\overline{K_2}$	$\overline{K_3}$	*R*	*f*	*S*	*V*	*F*
Austenitizing	673.2	700.5	728.2	55	2	4537.6	2268.8	2.4
Tempering	844	717.5	540.3	303.7	2	139603.7	69801.9	72.8
Cooling method	697.8	705.5	698.5	7.7	2	108.2	54.1	0.1
Error					2	1918.4	959.2	
Total					8	146167.9	$F_{0.05}(2,2)=19.0$	

Table 5 Orthogonal design analysis of elongation (EL)

Source	$\overline{K_1}$	$\overline{K_2}$	$\overline{K_3}$	*R*	*f*	*S*	*V*	*F*
Austenitizing	22.8	20.9	21.2	1.9	2	6.0	3.0	8.9
Tempering	19.9	20.6	24.3	4.4	2	33.7	16.9	50.4
Cooling method	21.1	21.5	22.3	1.2	2	2.1	1.1	3.2
Error					2	0.7	0.3	
Total					8	42.5	$F_{0.05}(2,2)=19.0$	

Table 6 Orthogonal design analysis of ductile-brittle transition temperature (DBTT)

Source	$\overline{K_1}$	$\overline{K_2}$	$\overline{K_3}$	*R*	*f*	*S*	*V*	*F*
Austenitizing	− 41.6	− 21.9	− 22.2	19.7	2	764.5	382.3	1.5
Tempering	− 13.7	− 34.7	− 37.4	23.7	2	1010	505	2.0
Cooling method	− 28.4	− 20.4	− 37	16.6	2	413.5	206.8	0.8
Error					2	515.8	257.9	
Total					8	2703.9	$F_{0.05}(2,2)=19.0$	

It is evident that tempering temperature is a significant factor on the $R_{p0.2}$ at a 95% confidence limit through *F*-test results in Table 4. So the most important influential factor on $R_{p0.2}$ is the tempering temperature. Austenitizing temperature and cooling method play negligible roles, which is consistent with the results based on *R* value analysis.

As shown in Table 5, F-value for tempering temperature is 50.4, which is more than $F_{0.05}$ (2, 2) = 19.0. Hence, tempering temperature play as more important role on the EL at a 95% confidence compared with austenitizing temperature and cooling method. The relative influence order is tempering temperature, austenitizing temperature and cooling method, which is the same as that on $R_{p0.2}$. However, austenitizing shows some extent influence on the EL of GN9 steel specimens.

From the *F* analysis in Table 6, it is evident that the relative influence order of heat treatment parameters on Charpy impact toughness (DBTT) is: tempering temperature, austenitizing temperature and cooling method. However, *F*-values for three heat treatment factors is lower than $F_{0.05}$ (2, 2) = 19.0. Fan et al. [33] suggested that the heat treatment parameters had a slight effect on the impact toughness of 1Cr12NiMo steel. The present work shows the similar results for GN9 steel.

The influence of three factors was re-evaluated from Figure 7. From Figure 7(a) and (b), it is evident found that the difference between the $R_{p0.2}$ and EL values at different levels of tempering temperature is more notable than that of the other two factors. From Figure 7(c), the difference between the DBTT values at different levels of tempering temperature is the most notable, which shows the similar trend as that by *R*-test in Table 6. However, the fluctuation of three factors for DBTT does not keep a monotone decreasing or increasing manner in Figure 7(c). It could be concluded that all three factors show some interactive effects on DBTT of GN9 steel.

4 Discussions

4.1 Heat Treatment on Tensile Properties

The strengthening mechanisms of 9%–12%Cr steels is classified into four categories, i.e., martensite transformation hardening, solution hardening, particle hardening and dislocation hardening. Martensite transformation

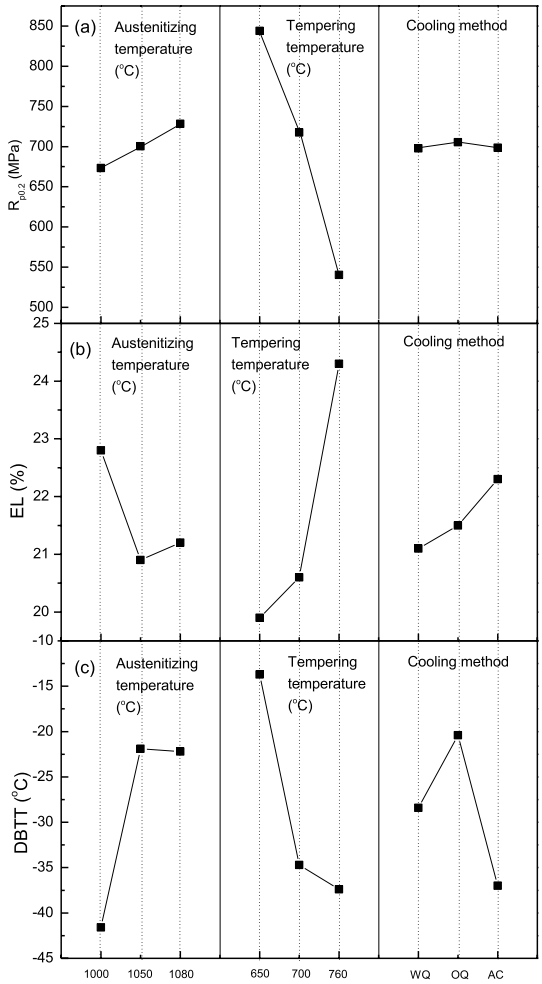

Figure 7 Effects of austenitizing temperature, tempering temperature, cooling method on (**a)** yield strength, (**b)** elongation and **c** ductile-to-brittle transition temperature

hardening and solution hardening are the main reasons for the favorable effect on yield and tensile strength of increasing austenitizing temperature. As mentioned in Section 3, the dissolution of carbides enhances the saturation of Cr, Mo and C in the matrix with the increasing of austenitizing temperature, which contributes to the solution hardening. Carbide dissolution also promotes the martensite transformation during austenization because the supersaturation of C causes an increase in the tetragonality of martensite [34]. As shown in Figure 2, the increasing austenitizing temperature show some favorable effects on reducing the lath width of GN9 steel, which also promote the increasing of room temperature strength.

During tempering, supersacturated C migrates from quenched martensite and forms $M_{23}C_6$ carbides and MX. The increment of tempering temperature promotes the precipitation of carbides, which lowers the hardening effects of martensite. The main microstructure of tempering specimens as shown in Figure 4 consists of tempered martensite. From Figure 5, it is evident that the dense of dislocation decreases with increasing tempering temperature at the same austenitizing temperature. On the other hand, $M_{23}C_6$ carbides are considered as the main obstacle for boundary movements and contribute to particle hardening. MX can pin the dislocation and improve the yield strength. However, the enhancement of carbide evolution to the strength seems limited compared with the reducing effects from the transformation of tempered martensite and the decreasing dislocation dense.

As shown in Table 3, the elongation of GN9 steel specimens after tempering at 650 °C or 700 °C is about 20% with the results increasing to 23%–26.5% after tempering at 760 °C. Compared with tempering temperature, the variation of austenitizing conditions has little influence on elongation. The main microstructural factors for elongation could be determined as dislocation dense through Figure 5.

4.2 Microstructural Aspects on Impact Toughness

The interactive effects between heat treatment parameters on impact toughness of GN9 steel should be attributes to their effects on the microstructural evolution. As for 9%–12%Cr FMS [2,5,16–20], the reported influential factors on DBTT could be listed as follows: prior austenite grains, lath width, carbide morphology and distribution, dislocation density.

The beneficial effect of fine grain in reducing the DBTT and increasing the USE is well known for ferritic/martensitic steels [35, 36]. As shown in Figure 2 the average prior austenite grain sizes vary within narrow limits, i.e., 8–12 μm. It could then be concluded that the prior austenite grain size is not the main factor for the variation of DBTT in GN9 steel specimens. Though lath widths decrease with the increasing austenitizing temperature, the upper shelf energy and DBTT are not improved as shown in Table 3.

As is known [37], inhomogeneous deformation occurs in interfaces between carbides and martensite matrix and dislocations concentrate around carbide particles under high strain rate (approximately 10^3 s^{-1} [38]) during Charpy impact testing. With the increasing of deformation, the accumulated dislocations and local deformation make the cohesion of interfaces weaken and microcracks form. The increasing amount of carbide sprovokes the microcrack formation and the subsequent propagation. However, the morphology and particle dimensions are the main factor which determines the propagation of microcracks [39, 40]. As proposed by Rolfe [41], the impact energy (K_V), fracture strength (K_{Ic}) and yield

strength ($R_{p0.2}$) could be expressed by Eq. (8). Habu and Rosenfiela [42] propose that the displacement (δ) of a microcrack tip equals to the adjacent distance (λ) of particles which make a microcrack propagates. The displacement (δ) and distance (λ) could be depicted by Eqs. (9) and (10), respectively:

$$K_V = \frac{K_{Ic}^2}{R_{p0.2}}, \tag{8}$$

$$\delta = \frac{K_{Ic}^2(1-\nu^2)}{2ER_{p0.2}}, \tag{9}$$

$$\lambda = (\frac{\pi}{6f})^{1/3} r, \tag{10}$$

where ν is a constant and equals to about 0.3, E is Young's modulus, f is the volume fraction of carbides, r is the average carbide size. The combination of Eqs. (8), (9) and (10) generates:

$$K_V = 1.77Erf^{-1/3}. \tag{11}$$

We could see from Eq. (11) that the Charpy impact energy is proportional to the particle size and inverse to the volume fraction of carbides. Compared with tempering at 650 °C and 700 °C, the carbide sizes at grain boundaries and lath boundaries increase obviously in specimens after tempering at 760 °C. And the proposed mechanism of carbides on impact toughness is illustrated in Figure 8. With the microcrack propagating along boundaries to the front of carbide, the crack tends to deviate along the interface of carbide and matrix instead of the cracking of carbides. The deviation makes the propagating length of microcracks increase. Energies for the microcrack propagation, therefore, increase, which represents the increasing absorbed energies during Charpy impact testing. From Figures 3 and 5, the amount of $M_{23}C_6$ in specimens tempered at 650 °C is low and the particle size is smaller, which lowers the upper shelf energy and raises the DBTT of steel specimens. With the tempering temperature up to 760 °C, the increments of carbide density and particle sizes in GN9 steel specimens show favorable effects on impact performance as shown in Table 3 and Figure 8.

Dislocation density has effects on Charpy impact toughness through influencing the yield strength. As suggested by Eq. (8), the higher the yield strength ($R_{p0.2}$), the lower the impact absorbed energy. With the decreasing test temperature from room temperature to − 110 °C, the increments of yield strength is more significant than that of fracture strength (K_{Ic}), which makes the DBTT increases. However, the fluctuation of DBTT does not keep a monotone decreasing or increasing manner in

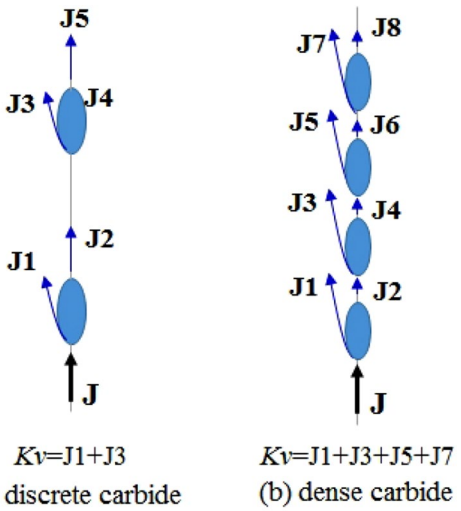

Figure 8 Mechanism of carbide effects on Charpy impact toughness of GN9 steel

Table 3 for different heat treatment conditions. Dislocation evolution during heat treatments, therefore, might not be the critical factor that has the same effects as $M_{23}C_6$ as mentioned above.

4.3 Optimal Heat Treatment Regime

As discussed above, the cooling method is not a significant factor for tensile properties of GN9 steel. From Figure 7, the optimum values of yield strength ($R_{p0.2}$) and elongation (EL) are obtained at the level of parameter C2 (oil quench) and C3 (air cooling), respectively. The Charpy impact toughness (DBTT) is minimum at the level of parameter C3 (air cooling). The optimal cooling method for GN9 steel is recommended to be air cooling after austenization.

From Figure 7, we could see that the highest yield strength, the maximum elongation and the lowest DBTT could be obtained when the austenitizing temperatures were chosen as A3 (1080 °C), A1 (1000 °C) and A1 (1000 °C), respectively. Though not be dissolved completely in the temperature range of 1000–1080 °C, carbides or carbonitrides are used to pin grain boundaries and decreasing the grain size. The undissolved $M_{23}C_6$ particles have little effect on tensile and impact properties of GN9 steel from Table 3. MX particles can pin the dislocation and hinder the dislocation movie, which enhance the strength of GN9 steel. Hence, the optimal austenitizing temperature is recommended to be lowered from 1050 °C [22–24] to 1000 °C.

From the analysis of Tables 4, 5 and Figure 7, the value of $R_{p0.2}$ decreased, while the value of EL increased with the increasing of tempering temperature. For getting good material properties on $R_{p0.2}$ and EL, tempering

temperature can be chosen B1 (650 °C) and B3 (760 °C), respectively. The value of $R_{p0.2}$ is 523.5 MPa when GN9 steel is temporized at 760 °C, which is sufficient to meet the demand of application ($R_{p0.2} \geq 490$ MPa). The value of DBTT is fittest when the tempering temperature was set at B3 (760 °C) from the aspect of microstructure examination. In order to achieve optimum combination of $R_{p0.2}$, EL and DBTT, tempering temperature is chosen as 760 °C.

Based on above analysis, the optimal heat treatment regime is austenitizing at 1000 °C for 0.5 h, followed by air cooling, and tempering at 760 °C for 1.5 h, followed by air cooling to room temperature.

5 Conclusions

The effect of heat treatment on the microstructure and mechanical properties of GN9 steel has been studied. The results obtained as follows:

(1) The microstructure of GN9 steel after orthogonal heat treatments consists of tempered martensite. The main precipitate is $M_{23}C_6$ carbides and MX carbonitrides. The distribution, morphology and amount of $M_{23}C_6$ are influenced by parameters of austenitizing and tempering treatments.

(2) The average prior austenite grain show sluggish growth tendency during austenization. The lath width decreases from 220–250 nm after austenization at 1000 °C to 180–190 nm after austenization at 1080 °C.

(3) With the increments of tempering temperature, dislocation density decreases. Austenitizing temperature and cooling methods have less influence on the dislocation evolution.

(4) Tempering temperature is the most important factor that influences the yield strength and elongation compared with austenitizing temperature and cooling methods. Austenitizing temperature, tempering temperature and cooling methods show interactive effects on impact toughness of GN9 steel from orthogonal design and analysis.

(5) Carbide morphology and distribution is the critical microstructural factor that influences the Charpy impact energy and DBTT of GN9 steel. Dense $M_{23}C_6$ carbides in discrete morphology could enhance the upper shelf energy and decrease the DBTT, while specimens with scarce, discrete and fine carbides at grain boundaries exhibit low shelf upper energy and high DBTT. The influence of prior austenite grains, lath width and dislocation density is not significant in the present study.

(6) Based on the orthogonal design and microstructural analysis, the optimal heat treatment of GN9 steel is proposed as follows: austenitizing at 1000 °C for 0.5 h followed by air cooling and tempering at 760 °C for 1.5 h.

Acknowledgements
The authors sincerely thanks to Dr. Wenjun Li and Dr. Jinming Liu for their assistance on SEM and TEM tests and the discussion of results.

Authors' Contributions
TM performed the experimental investigation and prepared the original draft; XH reviewed and edited the draft; PW assisted with analyses. All authors read and approved the final manuscript.

Authors' Information
Tingwei Ma, born in 1978, is currently a PhD candidate at *Key Laboratory of Electromagnetic Processing of Materials, Ministry of Education, Northeastern University, China*. He received his master degree from *Northeastern University, China*, in 2008. His research interests include nuclear materials.
Xianchao Hao, born in 1983, is currently an associate research fellow at *CAS Key Laboratory of Nuclear Materials and Safety Assessment, Institute of Metal Research, Chinese Academy of Sciences, China*.
Ping Wang, born in 1964, is currently a professor at *Key Laboratory of Electromagnetic Processing of Materials, Ministry of Education, Northeastern University, China*.

Funding
Supported by Natural Science Foundation Guidance Plan of Liaoning Province of China (Grant No. 2019-ZD-0362) and CAS Key Laboratory of Nuclear Materials and Safety Assessment, Institute of Metal Research, Chinese Academy of Sciences (Grant No. 2021NMSAKF02).

Availability of Data and Materials
Not applicable.

Declarations

Competing Interests
The authors declare no competing financial interests.

Received: 24 February 2021 Revised: 20 November 2023 Accepted: 23 November 2023
Published online: 19 December 2023

References

[1] X J Jin, S H Chen, L J Rong. Microstructure modification and mechanical property improvement of reduced activation ferritic/martensitic steel by severe plastic deformation. *Materials Science and Engineering A*, 2018, 712: 97-107.
[2] E H Jeong, J H Kim, S H Kim, et al. Influence of B and N on the microstructural characteristics and high-temperature strength of 9Cr-2W steel during and aging treatment. *Materials Science and Engineering A*, 2017, 700: 701-706.
[3] P Favuzza, A Aiello, M Cuzzani, et al. Erosion-corrosion resistance of reduced activation ferritic-martensitic steels exposed to flowing liquid lithium. *Fusion Engineering and Design*, 2018, 136: 1417-1421.
[4] L Tan, M A Sokolov, S J Pawel, et al. Varied enhancements in mechanical properties and sodium compatibility of Grade 92 by thermomechanical treatments. *Materials Science and Engineering A*, 2022, 832: 142359.
[5] X S Zhou, Y C Liu, C X Liu, et al. Austenitizing temperature effects on the martensitic transformation, microstructural characteristics, and mechanical performance of modified ferritic heat resistant steel. *Metallurgical and Materials Transactions A*, 2018, 49(8): 3525-3538.
[6] R L Klueh. Analysis of swelling behavior of ferritic/martensitic steels. *Philosophical Magazine*, 2018, 98: 2618-2636.

[7] P Yvon. *Structural materials for generation IV nuclear reactors*. London: Woodhead Publishing, 2017.
[8] P Shruti, T Sakthivel, G V S N Rao, et al. The role of themromechanical processing in creep deformation behavior of modified 9Cr-1Mo steel. *Metallurgical and Materials Transactions A*, 2019, 50(10): 4582-4593.
[9] A Prasitthipayong, D Frazer, A Kareer, et al. Micro mechanical testing of candidate structural alloys for Gen-IV nuclear reactors. *Nuclear Materials and Energy*, 2018, 16: 34-45.
[10] A Tiwari, R N Singh. Fracture behavior of ferritic/martensitic steels in DBT region characterized using CT and TPB specimen geometries. *International Journal of Fracture*, 2018, 209(1): 241-249.
[11] Y Dai, P Marmy. Charpy impact tests on martensitic/ferritic steels after irradiation in SINQ target-3. *Journal of Nuclear Materials*, 2005, 343(1-3): 247-252.
[12] R L Klueh, J J Kai, D J Alexander. Microstructure-mechanical properties correlation of irradiated conventional and reduced-activation martensitic steels. *Journal of Nuclear Materials*, 1995, 225: 175-186.
[13] D S Gelles. Microstructural examination of commercial ferritic alloys at 200 dpa. *Journal of Nuclear Materials*, 1996, 233(1): 293-298.
[14] C Y Yang, Y K Luam, D Z Li, et al. Effects of rare earth elements on inclusions and impact toughness of high-carbon chromium bearing steel. *Journal of Materials Science Technology*, 2019, 35(7): 1298-1308.
[15] J Parker, J Siefert. Metallurgical and stress state factors which affect the creep and fracture behavior of 9%Cr steels. *Advances in Materials Science and Engineering*, 2018, 2018: 6789563.
[16] E Aydogan, J G Gigax, S S Parker, et al. Nitrogen effects on radiation response in 12Cr ferritic/martensitic alloys. *Scripta Materilia*, 2020, 189: 145-150.
[17] E H Jeong, J H Kim, S H Kim, et al. Creep rupture chracteristics of cladding tubes of FC92B and FC92N: candidate alloys of SFR fuel cladding tube materials. *Metals and Materials International*, 2021, https://doi.org/10.1007/s12540-021-01031-5.
[18] S Pallaspuro, A Kaijalaineen, S Mehtonen, et al. Effect of microstructure on the impact toughness transition temperatures of direct-quenched steels. *Materials Science and Engineering A*, 2018, 712: 671-680.
[19] T W Ma, X C Hao, P Wang. Effect of heat treatments on Charpy impact properties of 15Cr12MoVWN ferritic/martensitic steel. *Journal of Iron and Steel Research International*, 2021, https://doi.org/10.1007/s42243-021-00616-z.
[20] J Y Choi, J Moon, J H Jang, et al. Enhancement of mechanical properties by repeated heat treatment in reduced activation ferritic/martensitic steel with Ta and Ti. *Journal of Nuclear Materials*, 2021, 557: 153321.
[21] J B Zhang, F Liu, D Fan, et al. Effect of heat treatment on delta-ferritie and impact toughness of P91 heat-resistant steel. *Transactions of Materials and Heat Treatment*, 2017, 38(4): 108-113. (in Chinese)
[22] K Tippey, P Jablonski, O Dogan, et al. Effects of alloying and processing modifications on precipitation behavior and elevated temperature strength in 9%Cr ferritic/martensitic steels. *Materials Science and Engineering A*, 2019, 756: 172-183.
[23] A Ganeev, M Nikitina, V Sitdikov, et al. Effects of the tempering and high-pressure torsoion temperatures on microstructure of ferritic/martensitic steel Grade 91. *Materials*, 2018, 11 (4): 627-636.
[24] General Administration of Quality Supervision, Inspection and Quarantine of the People's Republic of China: Standardization Administration of the People's Republic of China. GB/T 5310-2008 *Seamless steel tubes and pipes for high pressure boiler*. Beijing: China Standards Press of China, 2008. (in Chinese)
[25] C X Liu, D T Zhang, Y C Liu, et al, Investigation on the precipitation behavior of M_3C phase in T91 ferritic steels. *Nuclear Engineering and Design*, 2011, 241(7): 2411-2415.
[26] W B Jones, C R Hills, D H Polonis. Microstructural evolution of modified 9Cr-1Mo steel. *Metallurgical Transactions A*, 1991, 22(5): 1049-1058.
[27] O H Ibrahim, E S Elshazly. Microstructural effects on fracture behavior of ferritic and martensitic structural steels. *Journal of Materials Engineering and Performance*, 2013, 22(2): 584-589.
[28] R P B Ghasemi, M Yousefpour. The effect of one and double heat treatment cycles on the microstructure and mechanical properties of a ferritic steel. *Metallurgical and Materials Transactions A*, 2018, 49(3): 938-945.
[29] A Chatterjee, A Ghosh, A Moitra, et al. Role of hierarchical martensitic microstructure on localized deformation and fracture of 9Cr-1Mo steel under impact loading at different temperatures. *International Journal of Plasticity*, 2018, 104: 104-113.
[30] T S Byun, D T Hoelzer, J H Kim, et al. A comparative assessment of the fracture toughness behavior of ferritic-martensitic steels and nanostructured ferritic alloys. *Journal of Nuclear Materials*, 2017, 484: 157-167.
[31] S F Pugh, E A Little. *Proceeding of International Conference on Ferritic Steels for Fast Reactor Steam Generator*. London: British Nuclear Energy Society, 1978.
[32] A H Cai, Y Zhou, J Y Tan, et al. Optimization of composition of heat-treated chromium white cast iron casting by phosphate graphite mold. *Journal of Alloys and Compound*, 2008, 466(1-2): 273-280.
[33] R C Fan, M Gao, Y C Ma, et al. Effects of heat treatment and nitrogen on microstructure and mechanical properties of 1Cr12NiMo martensitic stainless steel. *Journal of Materials Science Technology*, 2012, 28(11): 1059-1066.
[34] A Khosravani, L Morsdorf, C C Tasan, et al. Multiresolution mechanical characterization of hierarchical materials: Spherical nanoindentation on martensitic Fe-Ni-C steels. *Acta Materialia*, 2018, 153: 257-269.
[35] Y Zhao, X Tong, X H Wei, et al. Effects of microstructure on crack resistance and low-temperature toughness of ultra-low carbon high strength steel. *International Journal of Plasticity*, 2019, 116: 203-215.
[36] M Balavar, H Mirzadeh. Enhancement of mechanical properties of low carbon steel based on heat treatment and thermo-mechanical processing routes. *Journal of Ultrafine Grained and Nanostructured Materials*, 2018, 51(2): 169-173.
[37] Z D Liu, Z Z Chen, H S Bao, et al. *Research and manufacturing of new type martensitic steel G115*. Beijing: Metallurgical Industry Press, 2020.
[38] C Y Gao, L C Zhang. A constitutive model for dynamic plasticity of FCC metals. *Materials Science and Engineering A*, 2010, 527(13-14): 3138-3143.
[39] L Pilloni, C Cristalli, O Tassa, et al. Grain size reduction strategies on Eurofer. *Nuclear Materials and Energy*, 2018, 17: 129-136.
[40] W Wang, X D Mao, S J Liu, et al. Microstructure evolution and toughness degeneration of 9Cr martensitic steel after aging at 550 °C for 20000 h. *Journal of Materials Science*, 2018, 53(6): 4574-4581.
[41] S T Rolfe, J M Barsom. *Fracture and fatigue control in structures, Application of Fracture Mechanics*. Upper Saddle River NJ: Prentice-hall, Inc., 1977.
[42] G T Hahn, M F Kanninen, A R Rosenfield. Fracture toughness of materials. *Annual Review of Materials Research*, 1972, 2: 381-404.